Hygro-elasticity and moisture diffusivity analysis of periodically heterogeneous materials by hierarchical microscale models

International Journal of Solids and Structures 273 (2023) 112231

Contents lists available at ScienceDirect

International Journal of Solids and Structures

journal homepage: www.elsevier.com/locate/ijsolstr

Hygro-elasticity and moisture diffusivity analysis of periodically heterogeneous materials by hierarchical microscale models

R. Masia, A.R. Sánchez-Majano, A. Pagani *

Mul2 Lab, Department of Mechanical and Aerospace Engineering, Politecnico di Torino, Corso Duca degli Abruzzi 24, 10129 Torino, Italy

ARTICLE INFO

Keywords:
Micromechanics
Moisture diffusivity
Hygro-elasticity
Unit cell
Mechanics of Structure Genome
Carrera Unified Formulation

ABSTRACT

The present paper focuses on developing a method to solve micromechanical analyses for the computation of moisture diffusivity and hygro-elastic characteristics of periodically heterogeneous materials and the recovery of the moisture flux and the stress over the Repeating Unit Cell (RUC). The model is based on the Mechanics of Structure Genome (MSG) to build a procedure capable of de-coupling the multiscale analysis into different steps on global and local levels, resulting in less demanding problems. On the other hand, the methodology uses the Carrera Unified Formulation (CUF) to engage a refined beam theory with high-fidelity capabilities. Hence, the longitudinal direction of the reinforcement is described with one-dimensional (1D) finite elements. Besides, for the cross-section, a hierarchical discretisation coupled with a non-isoparametric mapping technique allows reaching a high level of accuracy in the geometric description of the curvature of the fibre or inclusion. Finally, both hygro-elastic and moisture diffusivity problems are validated through numerical assessments showing excellent agreement with benchmarks in the literature.

1. Introduction

Composite materials are possibly involved in extreme environments, for instance, those characterised by extreme temperature gradients. Thus, there is a need to develop new efficient methods to predict the thermo-elastic properties directly, as shown in Yu and Tang (2007) and Sanchez-Majano et al. (2022). Another very aggressive environment for composite materials is one with high relative humidity, which leads to degradation of the materials in terms of the constitutive properties and strength (Pipes et al., 1976; Sih et al., 2012). Experiments are helpful in testing a particular wet environment's effects on materials, but these are not fully comprehensive for adequately understanding the nature of these changes. For this reason, it is necessary to develop models to understand the material behaviour thoroughly.

As long as the authors concern, not much work has been carried out in the field of modelling moisture diffusivity and hygro-elastic mechanics. For instance, Yuan and Zhou (2016) modelled the moisture absorption of unidirectional and 3D woven composites. Similarly, Laurenzi et al. (2008) studied the moisture diffusivity in carbon-braided composites, where a repetitive unit cell was developed for micro- and meso-scale simulations. Sinchuk et al. (2018) studied the moisture diffusion and induced swelling in carbon fibre textile composites by generating the numerical models by means of computed tomography. On the contrary, several works have been developed concerning the hygro-thermo-elastic analysis of composite structures. Instead of considering the hygro-thermo-elastic properties of the composite's constituents, these articles directly use homogenised properties from literature. For example, Patel, Ganapathi and Makhecha (Patel et al., 2002) studied the influence of the moisture concentration on the buckling load and natural frequency of thick composite plates. Likewise, Moleiro et al. (2019) and Moleiro et al. (2020) developed 3D exact solutions for the hygro-thermo-elastic analysis of multilayered plates and functionally graded materials.

The effective moisture diffusivity and effective hygro-elastic properties of composite material are strongly affected by the components' properties, the reinforcement volume fraction, their distribution, and orientation over the volume (Kondo and Taki, 1982; Bond, 2005). Different methodologies exist to predict hygroscopic features, namely analytical, semi-analytical and fully numerical. Among the former, one can refer to Hashin (1968), Springer–Tsai (Springer and Tsai, 1967) and Donea (1972). Indeed, these methods were originally oriented to calculate the thermal conductivity characteristics, but they can be employed with no further implications in the moisture diffusivity analysis due to the mathematical analogy between Fourier's law (Fourier, 1822) and the Fick's law (Fick, 1855) that govern the thermal and hygroscopic problem, respectively. The semi-analytical models are suitable for more generic cases. That is the case of the Method of Cells (MOC) (Aboudi, 1982), the Generalised Method of Cells (GMC) (Paley

* Corresponding author.
E-mail addresses: rebecca.masia@polito.it (R. Masia), alberto.racionero@polito.it (A.R. Sánchez-Majano), alfonso.pagani@polito.it (A. Pagani).

https://doi.org/10.1016/j.ijsolstr.2023.112231
Received 9 September 2022; Received in revised form 6 February 2023; Accepted 24 March 2023
Available online 23 April 2023

and Aboudi, 1992) and the High-Fidelity Generalised Method of Cells (HFGMC) (Aboudi et al., 2001). Last, fully numerical solutions can be provided by applying adequate boundary conditions to a Representative Volume Element (RVE) and then performing numerical analysis that replicates experimental methods, like stress or moisture diffusion tests (Sun and Vaidya, 1996; Kim and Ji, 2021).

The present work couples the Mechanics of Structure Genome (MSG), introduced by Yu (2016), with a well-established high order one-dimensional (1D) approach to solve the Repeating Unit Cell (RUC) problem. The concept of Structure Genome (SG) was introduced by Yu as the smallest building block of a structure and can represent different features depending on the studied structure. MSG relies on the Variational Asymptotic Method (VAM) (Berdichevskii, 1977), which allows for solving problems involving smaller parameters. This VAM characteristic is highly adequate for solving problems involving composites. Indeed, VAM is utilised to calculate the effective properties and local solutions of periodically heterogeneous materials through an asymptotic approach for the RUC problem in an efficient and accurate manner (Yu et al., 2012; Yu and Tang, 2007). On the other hand, we use 1D models to solve these demanding computational models by means of the Carrera Unified Formulation (CUF). CUF allows reducing general 3D problems into less computationally demanding 1D (Pagani and Sanchez-Majano, 2021; Pagani et al., 2021) and 2D (Sánchez-Majano et al., 2021; Pagani et al., 2022) models, while still retrieving highly accurate solutions. Arbitrary expansion functions can be used to characterise the cross-section and through-the-thickness direction for 1D and 2D problems, respectively, and generate numerical models that overcome the limitations of classical structural theories. Thus, a RUC can be represented by a 1D model whose axis is along the fibre or inclusion direction. The description of the geometry is carried out by an opportune coupling between Hierarchical Legendre Expansion (HLE) (Carrera et al., 2017a) with blending functions. By these means, a high-order non-isoparametric numerical model is obtained (Pagani et al., 2017a). In addition, the accuracy and validity of the proposed refined beam models for solving moisture diffusivity and hygro-elastic MSG problems will be demonstrated in the following chapters. Note that previous works dealt with the pure elastic and thermo-elastic micromechanical problems in de Miguel et al. (2017) and Sanchez-Majano et al. (2022), respectively. This manuscript is considered an extension of those articles.

The document is organised in the following sections: Section 2 depicts the moisture diffusivity problem in terms of the CUF-MSG formulation; then, the hygro-elastic problem is introduced in Section 3; afterwards, numerical assessments for both of the announced problems are reported in Section 4. Lastly, conclusions are drawn in Section 5.

2. Moisture diffusivity problem

An essential assumption for micromechanical analysis of the RUC is the consideration that the geometry, the boundary conditions and the different loading conditions referred to in the macroscopic scale do not affect the effective material properties of the RUC. Another fundamental point of the micromechanical formulation is that the local solutions have an average value over the RUC volume equal to the global solution of the macroscopic problem. Applying these hypotheses to the moisture diffusivity problem, one can write:

$$\frac{1}{V}\int_V \eta(\mathbf{x};\mathbf{y})dV = \bar{\eta}(\mathbf{x}) \tag{1}$$

where $\bar{\eta}$ represents the global moisture concentration field in the global reference system, $\eta(\mathbf{x};\mathbf{y})$ represents the local moisture concentration field that depends on both the global $\mathbf{x}$ and local $\mathbf{y}$ coordinates. V denotes the total volume on the unit cell. The present method uses two Cartesian coordinate systems: $\mathbf{x} = \{x_1, x_2, x_3\}$ and $\mathbf{y} = \{y_1, y_2, y_3\}$. $\mathbf{x}$ is used as the global reference frame of the macroscopic structure, whereas $\mathbf{y}$ is the local coordinate system describing the RUC. The origin of the local system is set at the centre of the RUC's face, as depicted in Fig. 1. Clearly, the longitudinal direction of the fibre coincides with the y_1-direction. The two reference systems are linked by the scaling parameter δ that characterises the small size of the RUC. In this regard, the relation between the two scales is $\mathbf{y} = \mathbf{x}/\delta$.

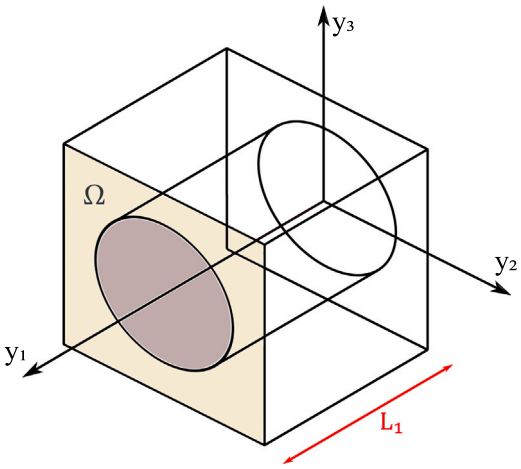

Fig. 1. Local coordinate system for RUC problem.

In view of the fact that continuous heterogeneous materials are formed by many unit cells, as illustrated in Fig. 2, it is necessary to ensure the boundary conditions on the RUC. Therefore, considering the edge lengths L_i, the continuity conditions of the moisture concentration field are applied as done in Yu and Tian (2007):

$$\begin{aligned}
\eta(x_1, x_2, x_3; 0, y_2, y_3) &= \eta(x_1 + L_1, x_2, x_3; L_1, y_2, y_3)\\
\eta(x_1, x_2, x_3; y_1, -L_2/2, y_3) &= \eta(x_1, x_2 + L_2, x_3; y_1, L_2/2, y_3)\\
\eta(x_1, x_2, x_3; y_1, y_2, -L_3/2) &= \eta(x_1, x_2, x_3 + L_3; y_1, y_2, L_3/2)
\end{aligned} \tag{2}$$

In the moisture diffusivity analysis, the local moisture concentration field, η can be expressed as the sum of the global moisture concentration field and a contribution representing the difference between both as:

$$\eta(\mathbf{x};\mathbf{y}) = \bar{\eta}(\mathbf{x}) + \delta\chi(\mathbf{x};\mathbf{y}) \tag{3}$$

where χ is the fluctuation function scaled with δ. By deriving the concentration field, the relation assumes the following form:

$$\eta_{,i}(\mathbf{x};\mathbf{y}) = \bar{\eta}_{,i}(\mathbf{x}) + \delta\chi_{,i}(\mathbf{x};\mathbf{y}) \tag{4}$$

where

$$\bar{\eta}_{,i}(\mathbf{x}) = \frac{\partial\bar{\eta}(\mathbf{x})}{\partial x_i} \qquad \chi_{,i}(\mathbf{x};\mathbf{y}) = \frac{\partial\chi(\mathbf{x};\mathbf{y})}{\partial x_i} + \frac{1}{\delta}\frac{\partial\chi(\mathbf{x};\mathbf{y})}{\partial y_i} \tag{5}$$

Thus, by substituting the two terms obtained in Eq. (5) into Eq. (4), the gradient of the moisture concentration field will become:

$$\eta_{,i}(\mathbf{x},\mathbf{y}) = \frac{\partial\bar{\eta}(\mathbf{x})}{\partial x_i} + \frac{\partial\chi(\mathbf{x};\mathbf{y})}{\partial y_i} \tag{6}$$

where the term $\delta\partial\chi/\partial x_i$ has been neglected, according to VAM (Berdichevskii, 1977).

In the MSG model, the solution to the stationary problem is obtained by minimising the difference between the energy of the heterogeneous and homogenised material, expressed as a functional as follows:

$$\Pi = \left\langle \frac{1}{2}D_{ij}\eta_{,i}\eta_{,j} \right\rangle - \frac{1}{2}D^*_{ij}\bar{\eta}_{,i}\bar{\eta}_{,j} \tag{7}$$

where the $\langle\rangle$ denotes the volume average. D_{ij} is the second-order tensor containing the components of the moisture diffusivity of the heterogeneous material, while $\eta_{,}$ represents the gradient of the moisture concentration field. The second term refers to the homogenised

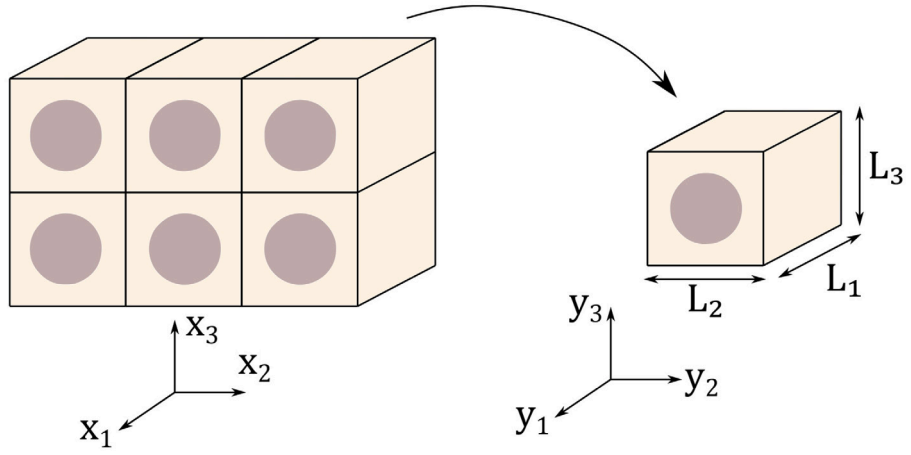

Fig. 2. Repeatable unit cells forming heterogeneous material.

material. Considering that the energy of the homogenised material is invariant, the second term in Eq. (7) can be discarded. The statement in Eq. (1) implies that $\bar{\eta}_{,i} = \langle \eta_{,i} \rangle$ and so that $\langle \chi_{,i} \rangle = 0$. Employing what is obtained in Eq. (6) into the first term of Eq. (7), one can rewrite the energy of the heterogeneous body in the form:

$$\Pi_1 = \left\langle \frac{1}{2} D_{ij} (\bar{\eta}_{,i} + \chi_{,i})(\bar{\eta}_{,j} + \chi_{,j}) \right\rangle \tag{8}$$

In the next section, high-order and geometrically accurate beam models are employed to solve the problem depicted in this section.

2.1. High-order beam models for the RUC problem

The classical beam theories ensure accurate results when dealing with slender structures in which the thickness segments remain perpendicular to the cross-sectional area and when the material is homogeneous. However, the situation described is not found in the RUC problem. Indeed, in this type of problem, the knowledge of the cross-section behaviour is crucial since different material phases might coexist in the numerical model. For these reasons, the introduction of higher-order models becomes essential since the high-order terms are able to capture the actual behaviour of complex models. MSG allows for solving the 2D problem, such as composites with fibre reinforcement, depicted in Fig. 1, or 3D problems, such as composites with particle inclusion. In this paper, CUF-based 1D models are employed to formulate the RUC problem in which the fluctuation unknowns, χ, are expanded over the cross-section $(y_2 - y_3)$ by means of arbitrary expansion functions, F_τ, as follows:

$$\chi(\mathbf{x}; y_1, y_2, y_3) = F_\tau(y_2, y_3)\chi_\tau(\mathbf{x}; y_1) \quad \tau = 1, \dots, M \tag{9}$$

where τ denotes summation, and M is the number of expansion terms adopted in the kinematic model. The accuracy of the model depends on the expansion functions chosen for the analysis, as demonstrated in previous works, see Sánchez-Majano et al. (2021) and Carrera et al. (2013). Several classes of expansion functions are available to define the F_τ, such as Taylor Expansions (TE), Lagrange Expansions (LE) and HLE. In the micromechanical analysis conducted in this work, HLE functions are employed since they combine the hierarchical features of the TE with the capability to interpolate the cross-section directly of the LE functions. Clearly, for the moisture diffusivity problem, the accuracy of the moisture concentration field is achieved simply by adding higher-order functions. Three types of function classes exist: vertex, side and internal, represented in Fig. 3. The vertex functions correspond to the first-order LE.

There are four vertex functions, one for each vertex. In order to capture the behaviour of the section edges, it is necessary to use at least a second-order function by adding the side expansions. Finally, the internal functions permit a complete description of the cross-section. In this manuscript, eighth-order HLE is the maximum polynomial order utilised for the CUF-MSG problem since it has been proven to be a sufficiently high order for a complete and accurate micromechanical analysis. Hereinafter, a specific HLE order will be written as HLn, where n is the order of the function. For instance, HL8 will indicate the use of eighth-order HLE. If the reader wills to deepen the HLE modelling, there exists more information available in Carrera et al. (2017b).

Refined beam theories exploiting higher-order expansions as HLE can be implemented by dividing the cross-section into different subdomains, each with its own HLE approximation, geometry, and material heterogeneity in the case of composite structures. It is clear that, due to the high polynomial orders employed for the kinematics, the discretisation of the physical domain should be as large as possible. Therefore, capturing the correct shape of the structural components with a minimum number of segments is necessary, which leads to the introduction of advanced mapping techniques for the expansion domains. The blending function method, introduced by Gordon and Hall (1973), enables one to include the exact shape of the cross-section by introducing parametric polynomials of an arbitrary order to describe the form of curved edges as shown in Fig. 4. The boundary surfaces of the domains are included directly in the mapping functions, $\boldsymbol{Q}$, and no geometrical error is introduced in the modelling procedure. Considering Fig. 4, the exact geometry of the fibre in the y_2y_3-plane is introduced into $\boldsymbol{Q}$ as:

$$\begin{aligned} y_2 &= Q_a(r,s) = \\ &\frac{1}{2}(1-s)a_1(r) + \frac{1}{2}(1+r)a_2(s) + \frac{1}{2}(1+s)a_3(r)\frac{1}{2}(1-r)a_4(s) - F_\tau(r,s)r_\tau \\ y_3 &= Q_b(r,s) = \\ &\frac{1}{2}(1-s)b_1(r) + \frac{1}{2}(1+r)b_2(s) + \frac{1}{2}(1+s)b_3(r)\frac{1}{2}(1-r)b_4(s) - F_\tau(r,s)s_\tau \end{aligned} \tag{10}$$

where $\tau = 1, \dots, 4$, and a_τ and b_τ are the parametric curves of the edges. Note that this approach cannot be considered iso-parametric since the mapping functions do not accord with the expansion functions, F_τ. The mapping allows us to reproduce the exact shape of complex section geometries using a minimum number of local expansions. Furthermore, the use of HLE mapping models reduces the error related to the geometrical approximation. This method is based on the seminal work of Szabó and Babuska (1991) and was first introduced by Pagani et al. (2017b) to curve the section of thin-walled beams. In the present paper, it is used to describe the exact geometries of the beam RUC cross-section with the curvature of the fibre or inclusion. The mapping procedure is used only in those subdomains where the presence of curvature is recorded. For instance, considering subdomain 4 in Fig. 4, the procedure is activated along the right edge. Thus, in subdomain 5, the mapping is used in all four edges.

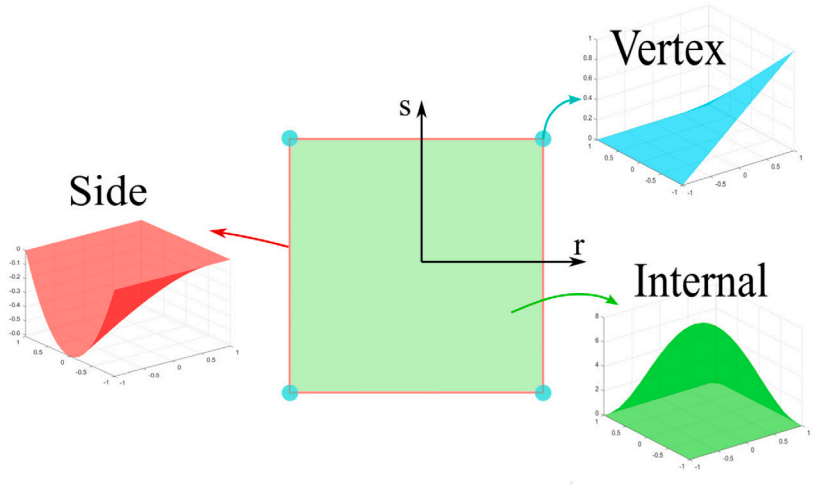

Fig. 3. Types of HLE expansion functions.

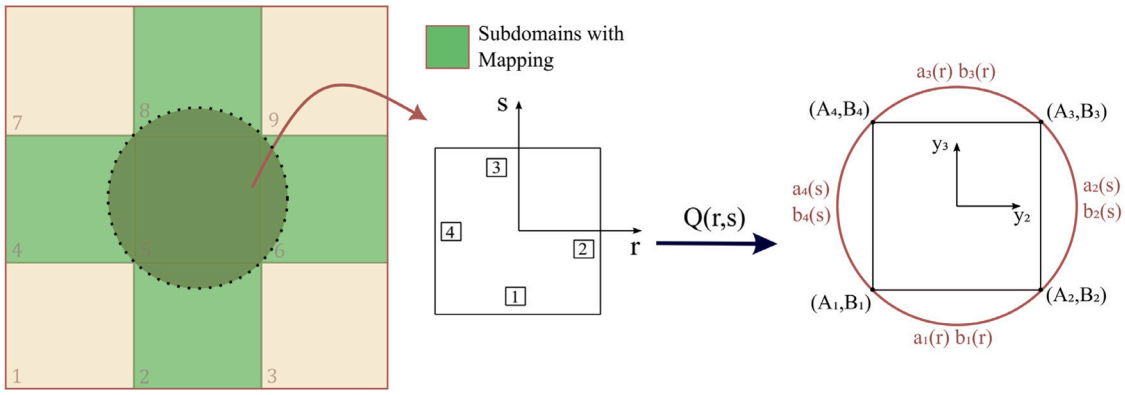

Fig. 4. Activation of mapping procedure on cross-section subdomains.

2.2. Finite element implementation

To solve the MSG-CUF problem, the Finite Element Method (FEM) is introduced. The fibre direction is modelled through one-dimensional elements and interpolated with classical Lagrangian shape functions in the beam coordinate y_1:

$$\chi_\tau(\boldsymbol{x}; y_1) = N_i(y_1)\chi_{\tau i}(\boldsymbol{x}) \qquad i = 1, 2, \dots, n \tag{11}$$

where $\chi_{\tau i}$ is the nodal unknown, and n the number of nodes in the beam model selected. At this point, it is possible to introduce the gradient vector of the global moisture concentration field as:

$$\bar{\boldsymbol{\eta}}_{,}^{T} = \{\bar{\eta}_{,1} \quad \bar{\eta}_{,2} \quad \bar{\eta}_{,3}\} \tag{12}$$

The local moisture gradient can be expressed as:

$$\boldsymbol{\eta}_{,} = \bar{\boldsymbol{\eta}}_{,} + \boldsymbol{B}\chi \tag{13}$$

with $\boldsymbol{B}$ being the 3×1 gradient differential operator, defined as:

$$\boldsymbol{B} = \begin{Bmatrix} \partial y_1 \\ \partial y_2 \\ \partial y_3 \end{Bmatrix} \qquad \partial y_i = \partial(\cdot)/\partial y_i \quad i = 1, 2, 3. \tag{14}$$

In this manner, Eq. (8) can be rewritten as:

$$\Pi_1^* = \frac{1}{2}\int_V (\bar{\boldsymbol{\eta}}_{,} + \boldsymbol{B}\chi)^T \boldsymbol{D}(\bar{\boldsymbol{\eta}}_{,} + \boldsymbol{B}\chi) dV \tag{15}$$

The moisture diffusivity matrix $\boldsymbol{D}$ in the general case of anisotropic material can be defined as:

$$\boldsymbol{D} = \begin{bmatrix} D_{11} & D_{12} & D_{13} \\ D_{12} & D_{22} & D_{23} \\ D_{13} & D_{23} & D_{33} \end{bmatrix} \tag{16}$$

Recalling that $\chi = F_\tau N_i \chi_{\tau i}$, and substituting into Eq. (15), one can obtain:

$$\Pi_1^* = \frac{1}{2}(\chi_{sj}^T M^{\tau sij} \chi_{\tau i} + 2\chi_{sj}^T \boldsymbol{D}_{h\eta}^{sj} \bar{\boldsymbol{\eta}}_{,} + \bar{\boldsymbol{\eta}}_{,}^T \boldsymbol{D}_{\eta\eta} \bar{\boldsymbol{\eta}}_{,}) \tag{17}$$

in which:

$$M^{\tau sij} = \int_\Omega \int_l (\boldsymbol{B}(F_s N_j))^T \boldsymbol{D} \boldsymbol{B}(F_\tau N_i) d\Omega dy_1$$

$$\boldsymbol{D}_{h\eta}^{\tau i} = \int_\Omega \int_l (\boldsymbol{B}(F_s N_j))^T \boldsymbol{D} d\Omega dy_1 \qquad \boldsymbol{D}_{\eta\eta} = \int_\Omega \int_l \boldsymbol{D} d\Omega dy_1 \tag{18}$$

Being $M^{\tau sij}$ and $\boldsymbol{D}_{h\eta}^{\tau i}$ the 1×1 and 1×3 fundamental nuclei (FN) of the RUC problem for hygroscopic analysis. They contain the basic information of the MSG model. Additionally, $\boldsymbol{D}_{\eta\eta}$ is the averaged moisture diffusivity over the RUC volume. The indices τ and s, denote the loop acting on the HLE expansion functions related to the cross-section, while i and j to the loop of the LE expansion functions of the beam model along the fibre axis. For details about assembling CUF-based finite elements, please refer to Carrera et al. (2014).

Applying VAM to Eq. (17), yields the solution that minimises the functional:

$$M^{\tau sij} \chi_{\tau i} = -\boldsymbol{D}_{h\eta}^{sj} \bar{\boldsymbol{\eta}}_{,} \tag{19}$$

The linearity of the problem imposes that $\chi_{\tau i}(\boldsymbol{x}) = \chi_{\tau i0}\bar{\boldsymbol{\eta}}_{,}(\boldsymbol{x})$, being $\chi_{\tau i0}$ a 1×3 array containing the fluctuation solution. Hence, Eq. (19) can be written as:

$$\boldsymbol{M}^{\tau sij}\chi_{\tau i0} = -\boldsymbol{D}^{sj}_{h\eta} \tag{20}$$

By solving Eq. (20), the effective moisture diffusivity properties of the corresponding homogenised composite material are found. Inherently, the energy in the transition between heterogeneous and homogeneous material remains unchanged. Substituting the linear system from Eq. (19) into Eq. (17), the effective moisture diffusivity tensor, $\boldsymbol{D}^*$, can be calculated as:

$$\boldsymbol{D}^* = \frac{1}{V}(\chi^T_{\tau i}\boldsymbol{D}^{sj}_{h\eta} + \boldsymbol{D}_{\eta\eta}) \tag{21}$$

where $\boldsymbol{D}^*$ is written as a 3×3 matrix.

At this point, the gradient of the local moisture concentration field can be derived simply by introducing $\chi = F_\tau N_i \chi_{\tau i}$ into the geometric relation from Eq. (13), obtaining:

$$\boldsymbol{\eta}_{,} = \bar{\boldsymbol{\eta}}_{,} + \boldsymbol{B}(F_\tau N_i \chi_{\tau i}) \tag{22}$$

Finally, the diffusivity flux can be derived through Fick's law (Fick, 1855):

$$\boldsymbol{J} = -\boldsymbol{D}\boldsymbol{\eta}_{,} \tag{23}$$

where the negative sign stands for the fact that the flux goes from high concentration areas to low concentration areas. $\boldsymbol{J}_i$ represents the diffusivity flux vector and has dimensions kg/(mm^{2}s), D_{ij} moisture diffusivity matrix whose coefficients have dimensions mm^2/s and $\boldsymbol{\eta}_{,j}$ is the vector containing the components of the moisture concentration gradient with dimensions (kg/mm^3)/mm.

Note that when the material is exposed to a moist environment, the parameter of interest is not the moisture concentration in its nondimensional form but the percent moisture content. The nondimensional form of the percent moisture content M, as shown in Moleiro et al. (2020) is calculated as:

$$\nabla M = \frac{W_{\text{moistmaterial}} - W_{\text{drymaterial}}}{W_{\text{drymaterial}}} \times 100 = \frac{\boldsymbol{\eta}_{,j}}{\rho_{dry}} \times 100 \tag{24}$$

where ∇M indicates the gradient of percent moisture content and ρ_{dry} represents the density of the homogenised material, which can be obtained by applying the mixture rule for the matrix and fibre/inclusion constituents. From Eq. (24) it is possible to derive the moisture concentration gradient $\boldsymbol{\eta}_{,j}$ to which a certain percent moisture gradient corresponds, so that the local moisture flux $\boldsymbol{J}_i$ can be found through Eq. (23).

3. Hygro-elastic problem

As mentioned above, one can reformulate the micromechanical problem to compute the hygro-elastic characteristics. In this case, it will be possible to derive the entire set of elastic features for the homogenised material, as was done by de Miguel et al. (2017), plus the coefficients of moisture expansion (CME), β. The reader can note that the problem is equivalent to the thermo-elastic case conducted by Sanchez-Majano et al. (2022), in which, in addition to the elastic characteristics, the thermal expansion coefficient of the homogenised material was computed. For a complete investigation of the problem, the reader is invited to consult (Sanchez-Majano et al., 2022). In the hygro-elastic problem, it is required to apply the compatibility of the deformation field between adjacent RUCs, as did with the moisture concentration field, for the moisture diffusivity in Eq. (2).

In this case, the functional that has to be minimised is composed of two parts; the strain energy of the heterogeneous material and the strain energy of the equivalent homogenised material:

$$\Pi = \frac{1}{2}\left\langle C_{ijkl}\varepsilon_{ij}\varepsilon_{kl} + 2\mu_{ij}\varepsilon_{ij}\gamma \right\rangle - \frac{1}{2}C^*_{ijkl}\bar{\varepsilon}_{ij}\bar{\varepsilon}_{kl} - \mu^*_{ij}\bar{\varepsilon}_{ij}\gamma \tag{25}$$

where the former term for both energy contributions represents the pure elastic part, and the latter refers to the coupling between the elastic and hygroscopic problems. $\langle\rangle$ denotes the volume average. C_{ijkl}, ε_{ij} and μ_{ij} are the fourth-order elastic tensor, the second-order strain and hygro-stress tensors, respectively. γ represents the difference between c, which is the actual moisture concentration, and c_0, the moisture concentration at which the material is stress-free. The moisture concentration is related to the moisture content percentage by the relation:

$$M(\%) = \frac{c}{\rho_{dry}} \times 100 \tag{26}$$

Besides, μ_{ij} represents the stress-moisture tensor expressed as:

$$\mu_{ij} = -C_{ijkl}\beta_{ij} \tag{27}$$

where β_{ij} is the second-order moisture expansion tensor. As done in the previous micromechanical analysis, one can express the strain component, including the fluctuation unknowns. Through this formulation, it is possible to compute the unknown fluctuation terms by minimising the following functional:

$$\Pi^* = \frac{1}{2}\left\langle C_{ijkl}\left[\bar{\varepsilon}_{ij} + \chi_{(i,j)}\right]\left[\bar{\varepsilon}_{kl} + \chi_{(k,l)}\right] + 2\mu_{ij}\left[\bar{\varepsilon}_{ij} + \chi_{(i,j)}\right]\gamma \right\rangle \tag{28}$$

It is convenient to write the strain vector as:

$$\boldsymbol{\varepsilon} = \bar{\boldsymbol{\varepsilon}} + \mathbf{D}\boldsymbol{\chi} \tag{29}$$

where $\bar{\boldsymbol{\varepsilon}}$ represents the global strain vector and $\mathbf{D}\boldsymbol{\chi}$ the differentiated fluctuation functions. The extended expression of the differential array is available in de Miguel et al. (2017). Then, Hooke's law relates stresses and strains for the hygro-elastic case as:

$$\boldsymbol{\sigma} = \mathbf{C}\boldsymbol{\varepsilon} + \boldsymbol{\mu}\gamma \tag{30}$$

where $\mathbf{C}$ is the 6×6 material array condensed from the fourth-order tensor C_{ijkl}, and $\boldsymbol{\mu} = -\mathbf{C}\boldsymbol{\beta}$ is the 6×1 condensed matrix from μ_{ij}. The functional in Eq. (28) can be rewritten as:

$$\Pi^* = \frac{1}{2}\int_V \left[(\bar{\boldsymbol{\varepsilon}} + \mathbf{D}\boldsymbol{\chi})^T\,\mathbf{C}\,(\bar{\boldsymbol{\varepsilon}} + \mathbf{D}\boldsymbol{\chi}) + 2\boldsymbol{\mu}(\bar{\boldsymbol{\varepsilon}} + \mathbf{D}\boldsymbol{\chi})\gamma\right] dV \tag{31}$$

Periodic boundary conditions of the RUC posing on the sides of the cross-section ($\chi^+_\tau = \chi^-_\tau$), and on the sections orthogonal to the fibre ($\chi_{\tau 1} = \chi_{\tau n}$) are applied. Then, introducing the CUF-FEM formulation of the fluctuation unknowns $\chi = F_\tau N_i \chi_{\tau i}$, the functional Π^* becomes:

$$\Pi^* = \frac{1}{2}\left(\chi^T_{sj}\boldsymbol{E}^{\tau sij}\chi_{\tau i} + 2\chi^T_{sj}\boldsymbol{D}^{sj}_{h\varepsilon}\bar{\boldsymbol{\varepsilon}} + \bar{\boldsymbol{\varepsilon}}^T\boldsymbol{D}_{\varepsilon\varepsilon}\bar{\boldsymbol{\varepsilon}} + 2\chi^T_{sj}\boldsymbol{D}^{sj}_{h\gamma}\gamma + 2\bar{\varepsilon}^T\boldsymbol{D}_{\varepsilon\gamma}\gamma\right) \tag{32}$$

where

$$\begin{aligned}
\mathbf{E}^{\tau sij} &= \int_\Omega\int_l (\boldsymbol{D}(F_s N_j \boldsymbol{I}))^T\boldsymbol{C}\boldsymbol{D}(F_\tau N_i \boldsymbol{I})d\Omega dy_1 \\
\mathbf{D}^{sj}_{h\varepsilon} &= \int_\Omega\int_l (\boldsymbol{D}(F_s N_j \boldsymbol{I}))^T\boldsymbol{C}d\Omega dy_1 \qquad \mathbf{D}_{\varepsilon\varepsilon} = \int_V \boldsymbol{C}dV \\
\mathbf{D}^{sj}_{h\gamma} &= \int_\Omega\int_l (\boldsymbol{D}(F_s N_j \boldsymbol{I}))^T\boldsymbol{\mu}d\Omega dy_1 \qquad \mathbf{D}_{\varepsilon\gamma} = \int_V \boldsymbol{\mu}dV
\end{aligned} \tag{33}$$

in which $\mathbf{I}$ is the 3×3 identity array. On the one hand, the 3×3 $\mathbf{E}^{\tau sij}$ matrix, the 3×6 $\mathbf{D}^{sj}_{h\varepsilon}$ matrix, and the 3×1 $\mathbf{D}^{sj}_{h\gamma}$ matrix are the fundamental nuclei (FN) of the hygro-elastic RUC structural problem, which contain the complete details about the structural problem. Furthermore, $\mathbf{D}_{\varepsilon\varepsilon}$ and $\mathbf{D}_{\varepsilon\gamma}$ are the averaged material stiffness matrix and averaged material hygro-stiffness matrix respectively. Note that the expansion functions F_τ are integrated on the cross-section area Ω, and the shape functions N_i are integrated along the longitudinal direction of the model l. Consequently, looping through the indexes τsij, one can calculate the assembled $\mathbf{E}$, $\mathbf{D}_{h\varepsilon}$ and $\mathbf{D}_{h\gamma}$ matrices for the RUC problem. The indices τ and s constitute the loop over the cross-sectional functions. For the sake of brevity, the extended expression of the matrices $\mathbf{E}^{\tau sij}$ and $\mathbf{D}^{\tau i}_{h\varepsilon}$ are not given in this article. However, these

can be consulted in the work of de Miguel et al. (2017), whereas the explicit form of $\mathbf{D}_{h\gamma}^{\tau i}$ is:

$$\begin{aligned}\boldsymbol{D}_{h\gamma 11}^{\tau i} &= \mu_{11}\int_l N_{i,y_1}dy_1\int_\Omega F_\tau d\Omega + \mu_{13}\int_l N_i dy_1\int_\Omega F_{\tau,y_3}d\Omega + \\ &\quad \mu_{12}\int_l N_i dy_1\int_\Omega F_{\tau,y_2}d\Omega \\ \boldsymbol{D}_{h\gamma 21}^{\tau i} &= \mu_{22}\int_l N_i dy_1\int_\Omega F_{\tau,y_2}d\Omega + \mu_{23}\int_l N_i dy_1\int_\Omega F_{\tau,y_3}d\Omega + \\ &\quad \mu_{12}\int_l N_{i,y_1}dy_1\int_\Omega F_\tau d\Omega \\ \boldsymbol{D}_{h\gamma 31}^{\tau i} &= \mu_{33}\int_l N_i dy_1\int_\Omega F_{\tau,y_3}d\Omega + \mu_{23}\int_l N_i dy_1\int_\Omega F_{\tau,y_2}d\Omega + \\ &\quad \mu_{12}\int_l N_{i,y_1}dy_1\int_\Omega F_\tau d\Omega\end{aligned} \tag{34}$$

The fluctuation unknowns that minimise the functional in Eq. (32) can be retrieved by solving the following linear system:

$$\mathbf{E}\boldsymbol{\chi} = -\mathbf{D}_{h\varepsilon}\bar{\boldsymbol{\varepsilon}} - \mathbf{D}_{h\gamma}\gamma \tag{35}$$

Then, assuming the fluctuation is linearly proportional to $\bar{\boldsymbol{\varepsilon}}$ and γ, i.e.:

$$\boldsymbol{\chi} = \boldsymbol{\chi}_0\bar{\boldsymbol{\varepsilon}} + \boldsymbol{\chi}_\gamma\gamma \tag{36}$$

and substituting it into Eq. (35), one can write the following linear system:

$$\begin{cases}\mathbf{E}\boldsymbol{\chi}_0 = -\mathbf{D}_{h\varepsilon} \\ \mathbf{E}\boldsymbol{\chi}_\gamma = -\mathbf{D}_{h\gamma}\end{cases} \tag{37}$$

where $\boldsymbol{\chi}_0$ and $\boldsymbol{\chi}_\gamma$ are the unknown vectors of the whole numerical model. Finally, substituting Eq. (36) in the functional from Eq. (31), one can formulate the following potential:

$$\Pi^* = \frac{1}{2}\bar{\boldsymbol{\varepsilon}}^T\boldsymbol{C}^*\bar{\boldsymbol{\varepsilon}} + \bar{\boldsymbol{\varepsilon}}^T\bar{\boldsymbol{\mu}}\gamma \tag{38}$$

where $\bar{\boldsymbol{\varepsilon}}$ represents the global strains, and:

$$\boldsymbol{C}^* = \frac{1}{\Omega}(\boldsymbol{\chi}_0^T\boldsymbol{D}_{h\varepsilon} + \boldsymbol{D}_{\varepsilon\varepsilon}) \qquad \bar{\boldsymbol{\mu}} = \frac{1}{\Omega}\left[\frac{1}{2}(\boldsymbol{D}_{h\varepsilon}^T\boldsymbol{\chi}_\gamma + \boldsymbol{\chi}_0^T\boldsymbol{D}_{h\gamma}) + \boldsymbol{D}_{\varepsilon\gamma}\right] \tag{39}$$

$\mathbf{C}^*$ is the effective purely elastic coefficients matrix of the equivalent material, and $\bar{\boldsymbol{\mu}}$ is the effective hygro-stress coefficients vector which is also influenced by the elastic part. Besides, $\boldsymbol{D}_{h\varepsilon}$, $\boldsymbol{D}_{\varepsilon\varepsilon}$, $\boldsymbol{D}_{h\gamma}$ and $\boldsymbol{D}_{\varepsilon\gamma}$ are the assembled arrays of their aforementioned FN.

It is clear that, through the following expression, the effective coefficients of the moisture expansion $\bar{\boldsymbol{\beta}}$ can be obtained:

$$\bar{\boldsymbol{\beta}} = -\boldsymbol{C}^{*-1}\bar{\boldsymbol{\mu}} \tag{40}$$

By reintroducing the fluctuation solutions into the geometrical and constitutive expressions, the local fields over the RUC can be directly derived. Consequently, as for the thermo-elastic problem, the local strains become:

$$\boldsymbol{\varepsilon} = \bar{\boldsymbol{\varepsilon}} + \boldsymbol{D}(F_\tau N_i\boldsymbol{\chi}) \tag{41}$$

Ultimately, using Hooke's law, one can recover the heterogeneous material's local stresses due to applying a strain field and a variation of the moisture concentration within the global structure.

$$\boldsymbol{\sigma} = \mathbf{C}\boldsymbol{\varepsilon} + \boldsymbol{\mu}\gamma \tag{42}$$

4. Numerical results

The following numerical assessments are conducted to validate the micromechanics method for the homogenisation procedure of the effective moisture diffusivity computation for composite materials and the prediction of the moisture flux distribution over the RUC volume. First, the homogenisation procedures are conducted, and the results are compared with some analytical formulations found in the literature. Subsequently, the dehomogenisation procedure for two different types of microstructure is performed, and the trends over the volume of the RUC are displayed. The analytical methods involved in the validation process were developed by Hashin (1968), Springer–Tsai (Springer and Tsai, 1967), and Donea (1972). All the formulae from the cited works refer to the thermal conductivity problem, which is mathematically equivalent to moisture diffusivity. The method proposed by Hashin (1968) is referred to the composites reinforced with particles. However, the Springer–Tsai method is suitable for the fibre-reinforced case. Donea introduced two different formulations for the particle and fibre cases. Lastly, the prediction capabilities of the CUF-MSG method for the hygro-elastic problem are demonstrated. The hygro-elastic analysis is formally equivalent to the thermo-elastic study carried out in Sanchez-Majano et al. (2022).

4.1. Moisture diffusivity results

4.1.1. Homogenisation

The first example reported concerns a fibre-reinforced composite material. The moisture diffusivity of the glass fibre is set to $D = 1.41 \cdot 10^{-9}$ mm^2/s, whereas the matrix in epoxy resin has $D = 1.41 \cdot 10^{-7}$ mm^2/s. Henceforth, this composite will be referred to as glass/epoxy. Because the diffusivity of the fibres is almost negligible compared to that of the matrix, the value is set as a hundredth of the matrix's diffusivity, according to Fan et al. (2019). The volume fraction of the fibres is set to $V_f = 0.6$, and the microstructure selected is a square-pack, representing a composite reinforced with a circular fibre, as illustrated in Fig. 5(a). When dealing with a square-pack and hexagonal-pack models representing the fibres inclusion, no material changes occur along the y_1-direction. Hence, one two-node 1D shape functions are enough to ensure an accurate discretisation of the longitudinal direction of the model. That is also because the moisture diffusivity trend results at most linear along the fibre direction. The cross-section is described by nine four-node 2D subdomains in which the mapping procedure is activated when the fibre curvature within the subdomain is recorded, as explained in de Miguel et al. (2017). The curvature features are perfectly captured using HLE, combined with the blending functions mapping technique. These particular functions allow the HLE domains to be adapted to the geometric characteristics of the model.

The first step is the computation of the effective moisture diffusivity of the equivalent homogenised material. Table 1 collects the results of the homogenisation procedure obtained with the CUF-MSG approach compared to the Springer–Tsai (Springer and Tsai, 1967), and the Donea (1972) methods. The first step is the computation of the effective moisture diffusivity of the equivalent homogenised material. Table 1 collects the results of the homogenisation procedure obtained with the CUF-MSG approach compared to the Springer–Tsai (Springer and Tsai, 1967), and the Donea (1972) methods. A perfect agreement between the Springer–Tsai analysis and the present approach is observed. Besides, the latter lays between Donea upper and lower bounds. It is noteworthy that when the HLE order increases, the numerical result does not change for the computation of D_{11}. This behaviour means that the second order of HLE has already achieved the convergence of the solution. The reason resides in moisture diffusion terms of the problem. The lack of the *shear-like* terms in the moisture diffusivity matrix can be seen by comparing the moisture diffusivity problem with the hygro-elastic one. The relevant increase of the solution to the convergence usually appears in the shear terms. Thus, in the present method, the second-order HLE is enough to obtain accurate results, gaining reduced computational cost and time for the analysis. It is clear that considering the transverse diffusivity, D_{33}, a slight change can be appreciated due to the fact that the HLE functions describe the cross-section and, in this case, second-order polynomials may not be sufficient to describe the fibre curvature accurately.

The second assessment is conducted with cubic particle-reinforced composites, comprising a carbon particle within a polyimide matrix, referred to as C/polyimide hereinafter. The particle-reinforced model

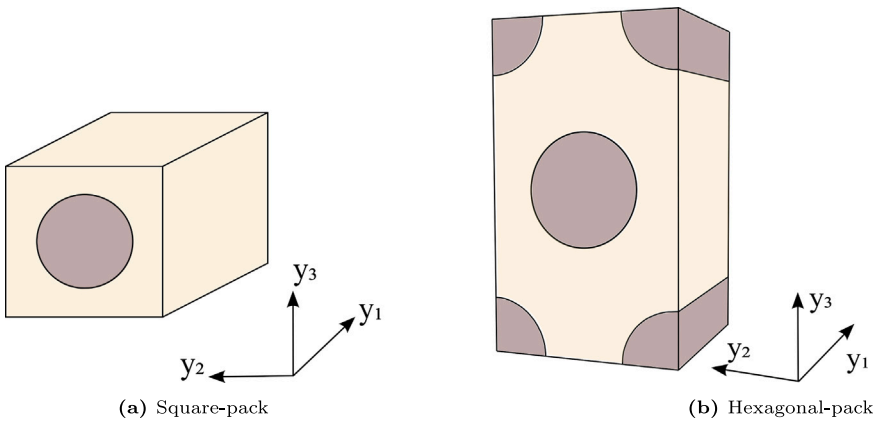

(a) Square-pack (b) Hexagonal-pack

Fig. 5. Microstructures models for fibre-reinforced composites.

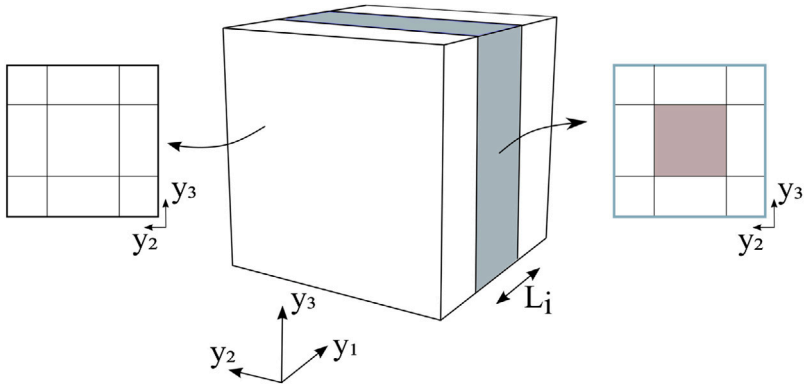

Fig. 6. Microstructure model for cubic particle-reinforced composites.

Table 1
Comparison of the effective longitudinal and transverse moisture diffusivity of fibre-reinforced glass/epoxy square-pack with $V_f = 0.6$. For the current approach, different HLE orders are considered.

Model	DOFs	$D_{11} \cdot 10^7$ [mm^2/s]	$D_{33} \cdot 10^7$ [mm^2/s]
Reference solutions			
Springer–Tsai (Springer and Tsai, 1967)	–	0.57	–
Donea lower bound (Donea, 1972)	–	0.52	–
Donea upper bound (Donea, 1972)	–	0.78	–
CUF-MSG			
HL2	80	0.57	0.36
HL4	194	0.57	0.34
HL6	380	0.57	0.34
HL8	630	0.57	0.34

is reported in Fig. 6. Material properties were obtained from Sinchuk et al. (2018). The moisture diffusion coefficient of the carbon reinforcement is negligible, and the diffusion of the matrix is set to $D = 2 \cdot 10^{-7}$ mm^2/s. For the particle inclusion microstructure, the longitudinal direction is described by six four-node 1D shape functions, that is, two FE per material constituent variation along the y_1-direction. The moisture diffusion is computed for different particle volume fractions and depicted in Fig. 7. The results of the present approach are compared to those obtained with Hashin upper bound (Hashin, 1968) and to the Donea formulation (Donea, 1972). Note the perfect match between the current approach and the Hashin method, while the Donea formulation overpredicts the moisture diffusivity for the cubic inclusion. As demonstrated in Shi et al. (2015), the value of the moisture diffusivity collapses when the fibre volume fraction increases.

Lastly, a fibre-reinforced glass/epoxy composite is taken into account. The microstructure selected is the hexagonal-pack, as shown in Fig. 5(b). The homogenisation procedure is performed for different fibre volume fractions, as shown in Fig. 8. Second-order HLE is selected since there was no variation between the values obtained with the eighth-order HLE order, as demonstrated previously for the glass/epoxy square-pack. A perfect agreement between the Springer–Tsai solution and the solution found with the present method is appreciated. On the contrary, the Donea upper bound overpredicts D_{11} for all the fibre volume fraction spectrum, while the lower bounds provides similar values when high fibre fractions are considered. For instance, when $V_f = 0.5$ Donea lower bound provides the values obtained with the present approach and Springer–Tsai method.

4.1.2. Dehomogenisation

In order to recover the local moisture flux between matrix and fibre into the composite, it is necessary to introduce the gradient of moisture concentration along the different directions of the fibre- or particle-reinforced composite. The following assessment recorded a gradient percentage of moisture equal to 30% in the y_1-direction for a C/polyimide particle reinforced composite. The composite has a cylindrical inclusion and a particle volume fraction equal to 0.35. Second-order HLE is selected to perform the analysis. Through Eq. (24), it is possible to obtain the moisture concentration gradient $\eta_{,y1}$=4.26 $\cdot 10^{-4}$ (g/mm^2)/mm, corresponding to a 30% gradient moisture. Six four-node elements along y_1-direction were used to discretise the direction of the fibre.

Fig. 9 shows the distribution of the y_1-moisture gradient over the fibre and the matrix. Note that the distribution is affected by the near-zero value of the moisture diffusion of the fibre. A large gradient

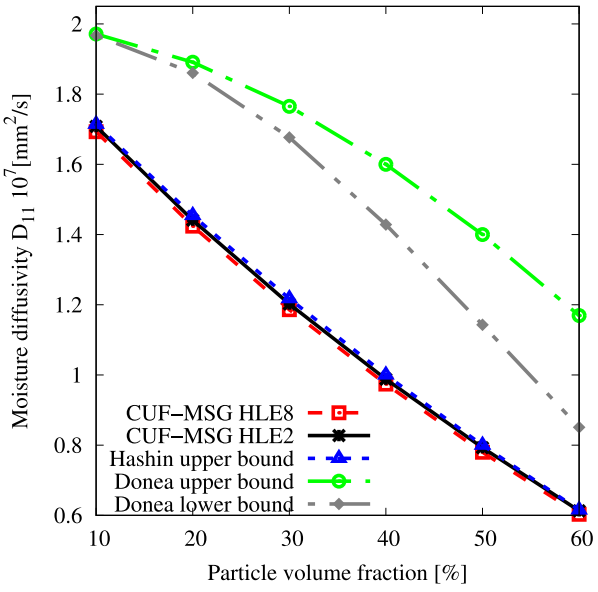

Fig. 7. Variation of the effective moisture diffusivity D of a cubic particle-reinforced C/polyimide composite with regard to the particle volume fraction. HLE orders selected are two and eight.

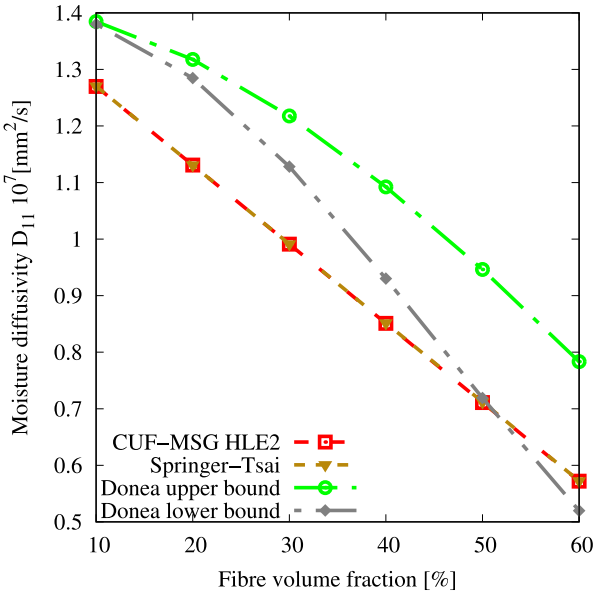

Fig. 8. Variation of the effective moisture diffusivity D of fibre-reinforced glass/epoxy hexagonal-pack with regard to the fibre volume fraction. HLE order selected is two.

variability is appreciated at the particle-matrix interface, where one order of magnitude and sign change is observed. The contour of the moisture flux in the longitudinal RUC direction, J_{11}, is displayed in Fig. 10. Again, large flux gradients are present within the RUC volume. This variability mainly takes place in the matrix constituent, where moisture absorption ($J_{11} > 0$) and moisture release ($J_{11} < 0$) occurs. The former happens in the central region of the RUC faces (y_1=0, L_1), whereas the latter appears in the regions closer to the inclusion. Conversely, the particle presents a constant moisture flux, one order of magnitude lower than that of the matrix. Although the flux is positive, the particle's moisture absorption can be neglected when compared to the matrix.

For the second evaluation, a glass/epoxy composite is considered. The microstructure selected is the hexagonal-pack. In this case, one

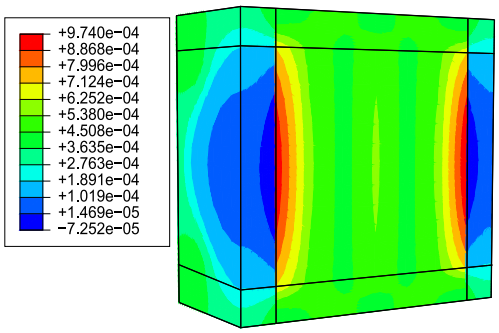

Fig. 9. Moisture gradient concentration $\eta_{,y1}$ over the cylindrical inclusion-RUC due to the moisture gradient of 30% along the y_1-direction for a C/polyimide particle reinforced composite, particle volume fraction 0.35, and second-order HLE.

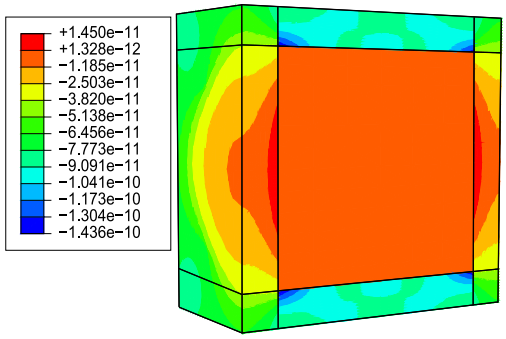

Fig. 10. Moisture flux J_{11} over the cylindrical inclusion-RUC due to the moisture gradient of 30% along the y_1-direction, for a C/polyimide particle reinforced composite, particle volume fraction 0.35 and second-order HLE.

two-node element is enough to describe the longitudinal direction while second-order HLE are used for the cross-section. The volume fraction is set to 0.30. First, a moisture concentration gradient of 30% along the y_1-direction was imposed in the model. Then, the same gradient is applied along the y_2-direction. For the first case, the contour of the flux in the fibre direction is displayed and its distribution is reported along the diagonal of the RUC's cross-section. As expected, constant values over the fibre and matrix subdomains are obtained when a longitudinal gradient is applied, as appreciated in Fig. 11(a). Moreover, the moisture flux over the fibre constituent is almost null as observed in Fig. 11(b). Fig. 12 provides the J_{22} contour and distribution along the RUC's cross-section when a 30% moisture concentration is applied in the y_2 direction. Concerning the former, high gradients are appreciated in the proximities of the fibre-matrix interfaces due to the differences in the moisture diffusivity tensor of both constituents. It is observed that the fibre absorbs moisture ($J_{22} > 0$) while the matrix is releasing it ($J_{22} < 0$). Nevertheless, the moisture absorbed by the fibre reinforcement is negligible compared to the matrix due to the large differences in terms of order of magnitude of the moisture diffusivity tensor. Note that despite the flux gradients over the RUC volume, second-order HLE are sufficient to capture an adequate distribution. This is due to the absence of *shear-like* terms when calculating the gradient of the moisture concentration field, $\boldsymbol{\eta}$,.

4.2. Hygro-elastic analysis

The hygro-elastic analysis allows us to compute the effective hygro-elastic properties. The analysis outputs are the homogenised material's elastic features and the three components of the moisture expansion tensor $\boldsymbol{\beta}$, referred to as CME.

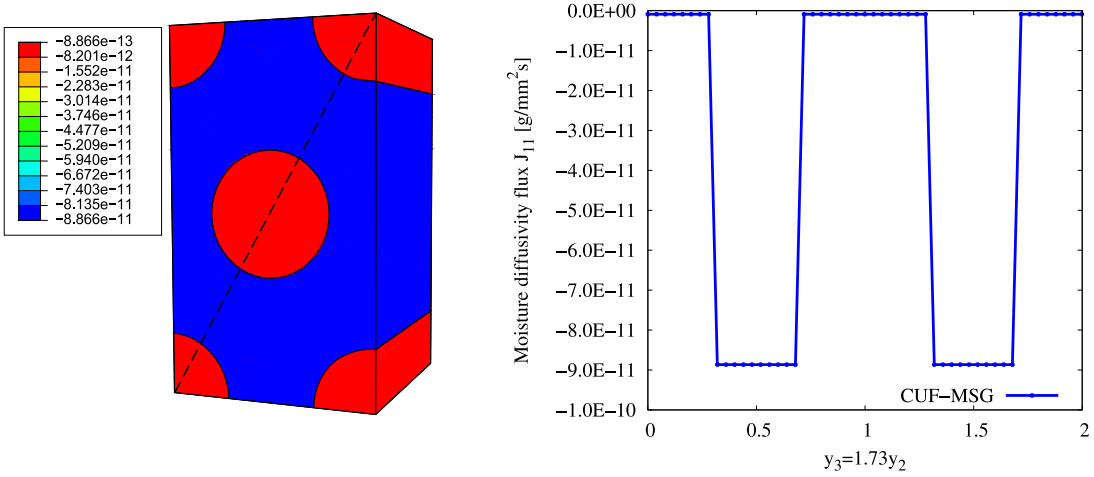

(a) J_{11} over the RUC volume **(b)** J_{11} along the diagonal

Fig. 11. Moisture flux J_{11} over the hexagonal-pack RUC due to the moisture gradient of 30% along the y_1-direction, for a glass/epoxy composite, fibre volume fraction 0.30 and second-order HLE.

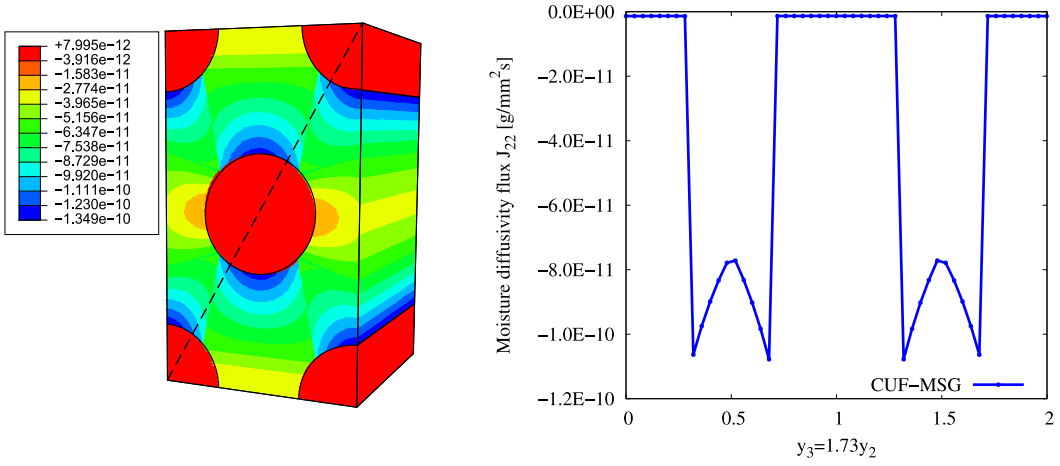

(a) J_{22} over the RUC volume **(b)** J_{22} along the diagonal

Fig. 12. Moisture flux J_{22} over the hexagonal-pack RUC due to the moisture gradient of 30% along the y_2-direction, for a glass/epoxy composite, fibre volume fraction 0.30 and second-order HLE.

A square-pack C/polyimide is first considered in order to validate the hygro-elastic micromechanical analysis. The hygro-elastic properties of both fibre and matrix are assumed to be isotropic. The hygro-elastic features of the carbon fibre are $E = 240$ GPa, $\nu = 0.2$ and, $\beta = 0$ $(g/m^3)^{-1}$, whereas the polyimide matrix has $E = 3.6$ GPa, $\nu = 0.3$ and $\beta = 1.86 \cdot 10^{-5}$ $(g/m^3)^{-1}$, which corresponds to 0.33 1/wt%. The complete hygro-thermo-elastic features of the C/polyimide composite are available in Sinchuk et al. (2018). In the validation process, different analytical and numerical methods are taken into consideration, such as Rosen and Hashin (1970), Reuss (Reuß, 1929), Voigt (1887), GMC (Paley and Aboudi, 1992), HFGMC (Aboudi et al., 2001) and MOC (Aboudi, 1982). All of these methods are collected from Aboudi, Arnold and Bednarcyk (Aboudi et al., 2021).

Fig. 13 provides the trend of the longitudinal and transverse CME against the fibre volume fraction. The present approach is compared to the aforementioned methods. A perfect agreement between the present approach and GMC, HFGMC and MOC is found in Fig. 13(a). On the contrary, the Voigt model overestimates β_1. This happens because Voigt's analytical method, as well as Reuss's method, does not consider the difference between the computation of longitudinal and transverse CME. Indeed, the values are higher than the other longitudinal CME but lower compared to the transverse results in Fig. 13(b). To better visualise that, the trend obtained by Voigt's method has also been plotted in the transverse CME graph in Fig. 13(b), highlighting the expected discrepancy. Note that the difference between Voigt's analytical solution and the one proposed in this manuscript is greater when lower fibre volume fractions are considered. Fig. 13(b) displays the trend of the transverse CME for different fibre fractions. As opposed to the longitudinal CME, discrepancies between CUF-MSG and GMC, HFGMC and MOC are found. Indeed, the latter methods provide higher values for β_2.

The MOC, GMC and HFGMC are semi-analytical methods in contrast with the CUF-MSG. The MOC is an approximate method based on the assumption that the two-phased composites have a periodic microstructure. GMC is based on the same premise, but it can be applied in more general cases, e.g. continuous composites. Simple geometry is studied in the present instance, so the same results are found for MOC and GMC. The HFGMC addresses the GMC's lack of shear coupling by employing a second-order displacement field instead of the GMC's first-order displacement field. For this reason, the values of HFGMC are slightly under the MOC and GMC's results. However, they are still closed.

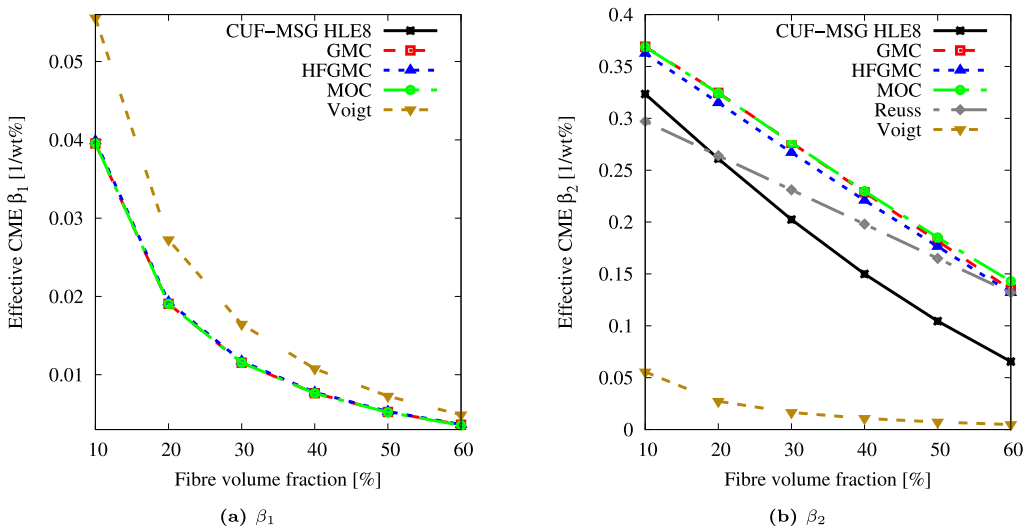

(a) β_1 (b) β_2

Fig. 13. Variation of the CMEs of fibre-reinforced composite C/polyimide square-pack with regard to the percentage fibre volume fraction. An HLE of eight order is used as expansion function in these plots.

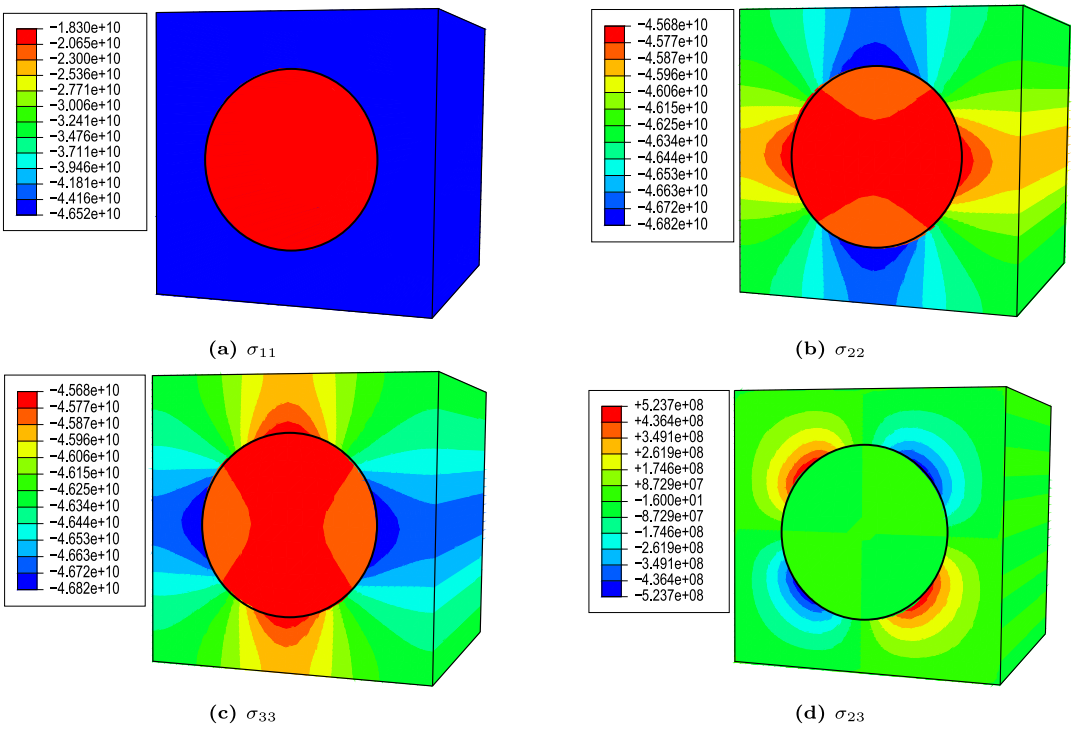

(a) σ_{11} (b) σ_{22}

(c) σ_{33} (d) σ_{23}

Fig. 14. Stress state due to a 20% moisture concentration increase/reduction over a C/polyimide square-pack. Stresses are reported in Pa. An eighth-order HLE is used for the cross-section.

Lastly, Reuss's model provides values closer to the considered semi-analytical methods, and perfectly matching with CUF-MSG when $V_f = 0.2$, and providing similar values to those of GMC, HFGMC and MOC when larger fibre fractions are considered.

Concerning the stresses retrieval, the square-pack stress state is calculated when a 20% moisture concentration along the y_1-direction is applied. A 30% fibre volume fraction is considered. The stress contours are shown in Fig. 14. Concerning the longitudinal stress component, σ_{11}, constant values are appreciated over the matrix and fibre domains, exhibiting both a compression character. Then, σ_{22} and σ_{33} present a similar distribution, rotated of 90 degrees, where high stress gradients are observed due to the mismatch in the moisture expansion coefficients β_{ij} tensor for both constituents. Last, the transverse shear component σ_{23} shows a doubly antisymmetric distribution.

5. Conclusions

In the current paper, an innovative 1D method has been employed to solve micromechanical moisture diffusion and hygro-elastic analyses. This method relies on the framework of the Carrera Unified Formulation (CUF) to develop high order FEs able to describe accurately composite materials mechanical behaviour. In detail, arbitrary expansions are used to approximate the problem unknowns on the cross-section, whereas FE approximations rely along the fibre/inclusion main direction. For the cross-section, a non-isoparametric mapping technique that employs HLE as expansion functions permits generating perfectly curved edges with no additional computational cost. Indeed, the degrees of freedom of the model increase when the HLE polynomial

order does. Following this approach, one is able to describe very complex geometries without necessarily increasing the computational costs. The CUF models were coupled with the Mechanics of Structure Genome (MSG) to solve the aforementioned moisture diffusivity and hygro-elastic analyses. In this manner, the effective moisture diffusivity tensor and the local moisture flux $\boldsymbol{J}$, in the moisture diffusivity analysis, as well as the effective coefficients of moisture expansion (CME) and the local stress distribution, for the hygro-elastic analysis, can be computed.

For the moisture diffusivity problem, the model has been validated through the comparison with some numerical benchmarks such as Donea, Springer–Tsai and Hashin analytical approaches, demonstrating the model's validity. Likewise, for the hygro-elastic procedure, the same models used for the thermo-elastic analysis (Sanchez-Majano et al., 2022) are involved in the current validation process, such as Reuss, Voigt, MOC, GMC, and HFGMC. The RUC models in the numerical assessment represented the classical fibre and particles reinforced composite that can be repeated over the volume to assemble most of the classical composite structures.

Furthermore, the proposed CUF+MSG micromechanical approach allows the computation of the homogenised material properties and the stress state, as well as moisture flux, in a single step analysis. This is advantageous compared to other micromechanical approaches, such as FE analysis, that tend to require several runs to calculate the aforementioned magnitudes.

The formulations presented can be adapted to numerous other problems, such as thermal conductivity. Moreover, as a future work, a fully hygro-thermo-elastic analysis might be performed by coupling the approach discussed in this manuscript with the one outlined in previous authors work (Sanchez-Majano et al., 2022). Besides, material non-linearities will be consider into the model to improve the simulation of the actual behaviour of composite materials.

Declaration of competing interest

The authors declare that they have no known competing financial interests or personal relationships that could have appeared to influence the work reported in this paper.

Data availability

Data will be made available on request.

Acknowledgements

This project has received funding from the European Research Council (ERC) under the European Union's Horizon 2020 research and innovation programme (Grant agreement No. 850437).

References

Aboudi, J., 1982. A continuum theory for fiber-reinforced elastic-viscoplastic composites. Internat. J. Engrg. Sci. 20 (5), 605–621.
Aboudi, J., Arnold, S.M., Bednarcyk, B.A., 2021. Practical Micromechanics of Composite Materials. Buttherworth-Heinemann, Oxford Spires Business Park, Kidlington, Oxforshire, United Kingdom.
Aboudi, J., Pineda, M.J., Arnold, S.M., 2001. Linear thermoelastic higher-order theory for periodic multiphase materials. J. Appl. Mech. 68 (5), 697–707.
Berdichevskii, V.L., 1977. On averaging of periodic systems. J. Appl. Math. Mech. 41 (6), 1010–1023.
Bond, D.A., 2005. Moisture diffusion in a fiber-reinforced composite: Part I – non-Fickian transport and the effect of fiber spatial distribution. J. Compos. Mater. 39 (23), 2113–2141.
Carrera, E., Cinefra, M., Petrolo, M., Zappino, E., 2014. Finite Element Analysis of Structures Through Unified Formulation. John Wiley and Sons, Ltd, Hoboken, New Jersey, USA.
Carrera, E., Filippi, M., Zappino, E., 2013. Laminated beam analysis by polynomial, trigonometric, exponential and zig-zag theories. Eur. J. Mech. A Solids 41, 58–69.
Carrera, E., de Miguel, A.G., Pagani, A., 2017a. Hierarchical theories of structures based on Legendre polynomial expansions with finite element applications. Int. J. Mech. Sci. 120, 286–300.
Carrera, E., de Miguel, A.G., Pagani, A., 2017b. Hierarchical theories of structures based on Legendre polynomial expansions with finite element applications. Int. J. Mech. Sci. 120, 286–300.
de Miguel, A.G., Pagani, A., Yu, W., Carrera, E., 2017. Micromechanics of periodically heterogeneous materials using higher-order beam theories and the mechanics of structure genome. Compos. Struct. 180, 484–496.
Donea, J., 1972. Thermal conductivities based on variational principles. J. Compos. Mater. 6 (2), 262–266.
Fan, Y., Gomez, A., Ferraro, S., Pinto, B., Muliana, A., la Saponara, V., 2019. Diffusion of water in glass fiber reinforced polymer composites at different temperatures. J. Compos. Mater. 53 (8), 1097–1110.
Fick, A., 1855. Ueber diffusion. Ann. Der Phys. 1 (94), 59–86.
Fourier, J.B.J., 1822. Théeorie analytique de la chaleur. pp. 1768–1830.
Gordon, W.J., Hall, C.A., 1973. Transfinite element methods: Blending-function interpolation over arbitrary curved element domains. Numer. Math. 21, 109–129.
Hashin, Z., 1968. Assessment of the self consistent scheme approximation: Conductivity of particulate composites. J. Compos. Mater. 2 (3), 284–300.
Kim, H.G., Ji, W., 2021. Thermal conductivity of a thick 3D textile composite using an RVE model with specialized thermal periodic boundary conditions. Funct. Composit. Struct. 3 (1), 015002.
Kondo, K., Taki, T., 1982. Moisture diffusivity of unidirectional composites. J. Compos. Mater. 16, 82–93.
Laurenzi, S., Albrizio, T., Marchetti, M., 2008. Modeling of moisture diffusion in carbon braided composites. Int. J. Aerosp. Eng. 2008.
Moleiro, F., Carrera, E., Ferreira, A.J.M., Reddy, J.N., 2020. Hygro-thermo-mechanical modelling and analysis of multilayered plates with embedded functionally graded material layers. Compos. Struct. 233, 111442.
Moleiro, F., Mota Soares, C.M., Carrera, E., 2019. Three-dimensional exact hygro-thermo-elastic solutions for multilayered plates: Composite laminates, fibre metal laminates and sandwich plates. Compos. Struct. 216, 260–278.
Pagani, A., Azzara, R., Carrera, E., 2022. Geometrically nonlinear analysis and vibration of in-plane-loaded variable angle tow composite plates and shells. Acta Mech. 1–24.
Pagani, A., Enea, M., Carrera, E., 2021. Quasi-static fracture analysis by coupled three-dimensional peridynamics and high order one-dimensional finite elements based on local elasticity. Internat. J. Numer. Methods Engrg..
Pagani, A., de Miguel, A.G., Carrera, E., 2017a. Cross-sectional mapping for refined beam elements with applications to shell-like structures. Comput. Mech. 59 (6), 1031–1048.
Pagani, A., de Miguel, A.G., Carrera, E., 2017b. Cross-sectional mapping for refined beam elements with applications to shell-like structures. Comput. Mech. 59.
Pagani, A., Sanchez-Majano, A.R., 2021. Stochastic stress analysis and failure onset of variable angle tow laminates affected by spatial fibre variations. Composit. Part C: Open Access 4, 100091.
Paley, M., Aboudi, J., 1992. Micromechanical analysis of composites by the generalized cells model. Mech. Mater. 14 (2), 127–139.
Patel, B.P., Ganapathi, M., Makhecha, D.P., 2002. Hygrothermal effects on the structural behaviour of thick composite laminates using higher-order theory. Compos. Struct. 56, 25–34.
Pipes, R.B., Vinson, J.R., Chou, T., 1976. On the hygrothermal response of laminated composite systems. J. Compos. Mater. 10 (2), 129–148.
Reuß, A., 1929. Berechnung der fließ grenze von mischkristallen auf grund der plastizitätsbedingung für einkristalle. ZAMM-J. Appl. Math. Mech./Zeitschrift FÜR Angew. Math. Und Mech. 9 (1), 49–58.
Rosen, B.W., Hashin, Z., 1970. Effective thermal expansion coefficients and specific heats of composite materials. Internat. J. Engrg. Sci. 8 (2), 157–173.
Sánchez-Majano, A.R., Azzara, R., Pagani, A., Carrera, E., 2021. Accurate stress analysis of variable angle tow shells by high-order equivalent-single-layer and layer-wise finite element models. Materials 14 (21), 6486.
Sanchez-Majano, A.R., Masia, R., Pagani, A., Carrera, E., 2022. Microscale themo-elastic analysis of composite materials by high order geometrically accurate finite elements. Compos. Struct..
Shi, Z., Zhigao, H., Yun, Z., Huamin, Z., 2015. Experimental investigation of moisture diffusion in short-glass-fiber-reinforced polyamide 6,6. J. Appl. Polym. Sci. 132, n/a–n/a.
Sih, G.C., Michopoulos, J., Chou, S.C., 2012. Hygrothermoelasticity. Springer Science & Business Media, Dordrecht, Netherlands.
Sinchuk, Y., Pannier, Y., Gueguen, M., Tandiang, D., Gigliotti, M., 2018. Computed-tomography based modeling and simulation of moisture diffusion and induced swelling in textile composite materials. Int. J. Solids Struct. 154, 88–96, Multiscale Modelling of Fibrous and Textile Materials.
Springer, G.S., Tsai, S.W., 1967. Thermal conductivities of unidirectional materials. J. Compos. Mater. 1 (2), 166–173.
Sun, C.T., Vaidya, R.S., 1996. Prediction of composite properties from a representative volume element. Compos. Sci. Technol. 56 (2), 171–179.
Szabó, B., Babuska, I., 1991. Finite Element Analysis. John Wiley and Sons, Ltd, Hoboken, New Jersey, U.S..
Voigt, W., 1887. Theoretische Studien über die Elasticitätsverhaltnisse der Krystalle. Abhandlungen Der Königlichen Gesellschaft Der Wissenschaften in Göttingen 34, 3–51.

Yu, W., 2016. A unified theory for constitutive modeling of composites. J. Mech. Mater. Struct. 379–411.
Yu, W., Hodges, D.H., Ho, J.C., 2012. Variational asymptotic beam sectional analysis - an updated version. Internat. J. Engrg. Sci. 59, 40–64.
Yu, W., Tang, T., 2007. A variational asymptotic micromechanics model for predicting thermoelastic properties of heterogeneous materials. Int. J. Solids Struct. 44 (22), 7510–7525.
Yu, W., Tian, T., 2007. A variational asymptotic micromechanics model for predicting thermoelastic properties of heterogeneous materials. Int. J. Solids Struct. 44 (22–23), 7510–7525.
Yuan, Y., Zhou, C., 2016. Meso-scale modeling to characterize moisture absorption of 3D woven composite. Appl. Compos. Mater. 23 (4), 719–738.